



LAWRENCE
LIVERMORE
NATIONAL
LABORATORY

Molecular mechanism of crystallization impacting calcium phosphate cements

J. L. Giocondi, B. S. El-Dasher, G. H. Nancollas,
C. A. Orme

June 2, 2009

PHILOSOPHICAL TRANSACTIONS OF THE ROYAL
SOCIETY A-MATHEMATICAL PHYSICAL AND
ENGINEERING SCIENCES

Disclaimer

This document was prepared as an account of work sponsored by an agency of the United States government. Neither the United States government nor Lawrence Livermore National Security, LLC, nor any of their employees makes any warranty, expressed or implied, or assumes any legal liability or responsibility for the accuracy, completeness, or usefulness of any information, apparatus, product, or process disclosed, or represents that its use would not infringe privately owned rights. Reference herein to any specific commercial product, process, or service by trade name, trademark, manufacturer, or otherwise does not necessarily constitute or imply its endorsement, recommendation, or favoring by the United States government or Lawrence Livermore National Security, LLC. The views and opinions of authors expressed herein do not necessarily state or reflect those of the United States government or Lawrence Livermore National Security, LLC, and shall not be used for advertising or product endorsement purposes.

Molecular mechanism of crystallization impacting calcium phosphate cements

Jennifer L. Giocondi¹, Bassem S. El-Dasher¹, George H. Nancollas², and Christine A. Orme^{1}*

¹Lawrence Livermore National Laboratory, Physical and Life Sciences, 7000 East Ave., Livermore, CA 94550, U.S.A

² Department of Chemistry, Natural Sciences Complex, University at Buffalo, The State University of New York, Buffalo, NY 14260, USA

* Corresponding author (orme1@llnl.gov)

Introduction	2
Experimental Methods	5
Substrate preparation using gel crystal growth	5
Electron backscattered diffraction (EBSD) to identify step directions	6
In-situ atomic force microscopy (AFM) to measure step kinetics	6
Solution Speciation	7
Results and Discussion	9
Step and surface structure	9
Impact of structure on processing	12
Step kinetics	13
The relationship between hillock geometry and crystal parameters	14
Dissolution behavior of brushite	15
Growth behavior of brushite without additives	15
Step anisotropy	17
Influence of additives on brushite growth	17
The impact of magnesium on brushite growth	17
The impact of citrate on brushite growth	19
The impact of oxalate on brushite growth	21
The impact of bisphosphonate on brushite growth	22
Conclusion and Outlook	24
Acknowledgements	26
Tables	27
Figure captions	29
References	31

Introduction

The biomineral, calcium hydrogen phosphate dihydrate ($\text{CaHPO}_4 \cdot 2\text{H}_2\text{O}$), commonly known as brushite and often denoted as DCPD, is a malleable material that both grows and dissolves readily. Compared to the other calcium phosphate (CaP) phases, it has a comparatively fast nucleation rate as a result of its low surface energy. It is also less stable than the other CaP phases at physiological pH. Within the body these properties can play a role in certain diseases, most notably in kidney stone formation where crystals form under mildly acidic conditions found in urine. However, these same properties, along with brushite's excellent biocompatibility, can be used to great benefit in making resorbable biomedical cements. This paper describes findings from crystal growth experiments on brushite. To put these experiments in context, we use the synthesis of calcium phosphate cements as an example of how this kinetic data might be used to impact formulation and processing. We begin with a brief description of how CaP cements are made pointing out desired processing goals and, in particular describing, which aspects of this problem might be aided by optimizing brushite crystallization conditions.

There are many processing challenges associated with optimizing calcium orthophosphate cements (Dorozhkin, 2008). These begin with the formation of the cements themselves. Cements are either high or low viscosity pastes that can be molded or injected into wound sites. They are synthesized by forming a viscous slurry from calcium phosphate powders mixed with a solvent. Typically two or more calcium phosphate species are reacted together to form either an apatite or brushite cement. The solvent is chosen such that the powders dissolve to form a supersaturated gel that eventually precipitates to form a solid composed of interlocked crystals. Brushite is of interest in both cement types - as an intermediate, in the formation of calcium deficient hydroxylapatite (CDHA) cements and, as a product, in the formation of brushite (DCPD) cements.

During this precipitation process it is important to control crystallization kinetics, the final crystal phase, the porosity, and the microcrystalline structure (Bohner, 2007). Together these properties affect the performance of the implant by influencing the setting

time, the mechanical characteristics, and the resorption rate. For example, the setting time must be slow enough to allow the surgeon time to inject the material while it is still pliable, but fast enough to provide mechanical integrity to the wound. For this reason it is important to control the nucleation and growth kinetics that initiate solidification. Similarly, the phase, the porosity, and the microstructure all affect the mechanical strength and can be tuned to some degree to suit the application.

Once the implant has been formed, it must be resorbed into the body. Ideally the resorption is balanced by bone growth to maintain mechanical strength at the wound site. Tuning the resorption rate is a complicated problem that depends both on the implant properties, such as phase and porosity, as well as the local biological processes. At the wound site, the local biochemistry is constantly evolving due to the body's inflammatory response and cellular activity. Proteins adsorb to the implant surface altering its interfacial properties. In addition, transport in and out of the porous structure can be limited, which causes heterogeneities and concentration gradients throughout the structure. Within these temporally and spatially varying surroundings, the calcium phosphate material responds to its locale by dissolving or, in some cases, changing phase. While this process cannot yet be fully controlled, it is of general interest to be able to slow or speed the dissolution of the calcium phosphate material under a range of conditions.

The setting time and the resorption time are important timescales that dictate many of the desired goals associated with crystallization kinetics (Figure 1). The setting time, which typically needs to be a few minutes, is the time that it takes to progress from a mixed paste to a solid, sufficiently rigid to hold its shape. This includes several stages from the dissolution of the starting materials to create a gel, the lag time before the onset of nucleation, and the time needed to grow an interpenetrating network of crystals. For this reason, the setting time can be influenced by altering the dissolution rate of the reactants or by slowing the nucleation and growth of the products or intermediates. In both cement types it is generally desirable to slow the nucleation and growth of DCPD crystals as this leads to the initial solidification of the gel and limits the surgeon's working time. There are several strategies for achieving this including the use of different solvents, the use of additives that can either inhibit nucleation or alter growth rates and

the variation of crystal growth parameters such as the supersaturation, the ionic strength, or the ratio of calcium to phosphate.

The resorption time is dictated by the biological and chemical environment as well as implant properties such as porosity, solubility and stability. Of these factors, the solubility and material stability, can be modified by altering brushite's inherent interfacial kinetics. Brushite is undersaturated in healthy physiological settings (Orme and Giocondi, 2007a). For this reason, brushite will either dissolve or convert to apatite over time. The inherent dissolution of brushite can be influenced both by particle size (Tang *et al.*, 2003) as well as additives. The conversion of brushite to less soluble apatite is an essential step in the formation CDHA cements, but is typically undesirable for brushite cements because it slows the resorption rate. For this reason, additives that influence the removal of water are of interest for DCPD cements. Magnesium ions (Lilley *et al.*, 2005) and pyrophosphate (Grover *et al.*, 2006) have been demonstrated to inhibit the hydrolysis reaction thereby lessening CDHA formation and the associated decrease in resorption rate.

Recent reviews (Bohner, 2007) have laid out a framework, summarized in Figure 1, to connect molecular mechanisms of crystallization with aspects of process control. This paper continues along these lines, focusing on the interfacial physics at brushite surfaces that may impact the processing and evolution of calcium phosphate cement materials. Although, dissolution is briefly discussed, the primary focus is on growth.

To address questions of how solution parameters, solvents and impurities alter brushite kinetics we have employed scanning probe microscopy (SPM) as a means of monitoring both the morphology and kinetics of atomic step motion. Brushite crystals are highly heterogeneous with multiple facets and several steps on each face. Unlike bulk studies, SPM results are not averaged over different step directions or different facets that each may interact with additives in unique ways. For this reason, SPM has been particularly useful in advancing the science of impurity interactions.

Because it is often interactions at step-edges (as opposed to facets) that serve as the molecular docking sites for growth modifiers (Tang *et al.*, 2001; Qiu *et al.*, 2005), ascertaining step structure is fundamental to SPM studies. We use electron back-scattered diffraction (EBSD) to provide positive identification of the step directions, which

historically have been identified by either macroscopic morphology (Ohta *et al.*, 1979) or by high-resolution atomic force microscopy (Scudiero *et al.*, 1999; Kanzaki *et al.*, 2002). Our results confirm previous identifications, but utilize a more reliable methodology.

In what follows we will briefly discuss brushite growth and dissolution in solutions without additives to provide a baseline. Kinetic data will suggest that HPO_4^{2-} , rather than Ca^{2+} , incorporation is the rate-limiting step during growth. This may suggest a means to slow growth rate without additives. We will also describe the effect of three additives that have been used to alter DCPD cements: magnesium ions, citrate, and the bisphosphonate, etidronate. We also compare citrate, which has three carboxyl groups with oxalate, which has two. In general, images are used to indicate which surface steps interact with the additive and step kinetics are used to provide additional information on mechanism. Results show that magnesium slows the growth rate of all brushite steps. By contrast, citrate has little effect on the step kinetics but lowers the density of steps on the surface. Oxalate has similar effects on kinetics, but stabilizes a facet not observed in the presence of citrate. On the other hand etidronate binds specifically to polar steps and substantially increases the kinetics of non-polar steps.

Experimental Methods

Substrate preparation using gel crystal growth

Brushite crystal substrates were grown in 1 wt% agarose gels (low melt, Pierce) by the single diffusion method using $\text{CaCl}_2 \cdot 2\text{H}_2\text{O}$ (EM Science, 99.5%) and KH_2PO_4 , KDP, (ProChem, 99.999+%) as the calcium and phosphate sources respectively. The stock solutions of each reagent were filtered using a 0.2 μm PTFE filter prior to use. 0.1M KDP was added to the gel phase and the top solution contained 0.1M $\text{CaCl}_2 \cdot 2\text{H}_2\text{O}$. The final pH of both the gel phase and the top solution were adjusted to 5. The gel was allowed to set for 24 hours before adding the top solution and the vials were incubated at room temperature. The crystals were harvested from the gels, rinsed in water and dried and stored on ashless filter paper. The phase and chemistry of the substrates were validated by both powder x-ray diffraction (XRD) and Raman spectroscopy.

Electron backscattered diffraction (EBSD) to identify step directions

EBSD was used to determine the surface orientation and the crystallographic directions that corresponded to etch pit edges as view by AFM. To determine crystallite orientation, a Tex SEM Laboratories, Inc EBSD system integrated with an FEI Instruments Quanta 200 environmental scanning electron microscope (ESEM) was used. The crystals were examined without any conductive coating, and the microscope was run at 20 kV in low vacuum mode with a water vapor pressure of 0.5 torr to help minimize charging. Individual diffraction patterns were collected by rastering the beam over small areas ($\sim 5 \mu\text{m} \times 5 \mu\text{m}$) on the crystal surface instead of the typical collimating of the electron beam onto a spot, as this was discovered to locally charge up the crystal and lead to poor diffraction and cracking. The collected diffraction patterns were then indexed to determine the crystallite orientations.

In-situ atomic force microscopy (AFM) to measure step kinetics

In-situ AFM was used to observe the crystal growth from dislocation hillocks on the $\{010\}$ surface of platelet-like, gel grown brushite crystals. Crystals were anchored with a UV-curable adhesive (UV15, Masterbond) and freshly cleaved prior to imaging in solution using an atomic force microscope (Nanoscope III, Digital Instruments, Santa Barbara, CA) equipped with a commercially available flow-through fluid cell. Solution flow rates (1.0-1.5 mL/min) were chosen such that step growth kinetics were not limited by bulk diffusion. The solution temperature entering the fluid cell was maintained at 37 °C by keeping the solution reservoir in an incubator at 40 °C and resistively heating the tubing leading from the incubator to the fluid cell to reduce cooling losses in the tubing. The fluid cell temperature was measured using a 0.005" diameter Copper-Constantan thermocouple (Omega) fitted to the outlet of the fluid cell.

All images are $2\mu\text{m} \times 2\mu\text{m}$ and were acquired in contact mode using Si_3N_4 tips. The force between the tip and the sample was reduced to the minimum possible value that allowed the tip to remain in contact with the surface and did not have a measurable effect on the growth kinetics. Note that step-angle distortion exists in the images because the step front advances during the scan time. Images reported here are not corrected for

this effect. Instead, the change in step angle in images acquired in scanned up and scanned down images was used to provide a measure of both the true step angle and the step velocity as given by the equations:

$$\tan \varphi_0 = \frac{4x_{pix}m_u m_d + m_u + m_d}{2[x_{pix}(m_u + m_d) + 1]} \quad (1)$$

$$\frac{v}{v_{tip}} = \frac{m \cos(\varphi_0) - \sin(\varphi_0)}{2x_{pix}m + 1}$$

where m_i is the apparent slope of the step in up (m_u) and down (m_d) scanned images, $\tan(\varphi_0) = m$ is the true slope of the step, v is the true velocity of the step, x_{pix} is the number of pixels per line, and v_{tip} is the velocity of the tip in pixels per second given by $v_{tip} = 2(scan\ rate)(scan\ size)$. All images were processed and analyzed with Image SXM (v1.81). In cases where solutions with different concentration conditions were exchanged, measurements were made using images acquired at least 3 minutes after the exchanges occurred to insure that the new solution had equilibrated in the fluid cell. With a fluid cell volume of approximately 50 μ L, this equilibration time is sufficient to refill the fluid cell more than 50 times with the flow rates used.

Solution Speciation

Solutions for AFM experiments were prepared making “A” and “B” solutions by the introduction of filtered (0.2 μ m PTFE filter) stock solutions. The “A” solution contained NaCl and CaCl₂·2H₂O and the “B” solution contained KDP and KOH. The “B” solution was then slowly added to the “A” solution while stirring, the temperature was adjusted to 37 °C, and the pH was adjusted by slow addition of 0.1M KOH.

The base solutions used consisted of two formulations, the components of which are shown in Table 1. These values all fall within range of concentrations found in human urine (Orme and Giocondi, 2007a). The supersaturation ratio, S , with respect to brushite is defined as:

$$S = \frac{a\{Ca^{2+}\}a\{HPO_4^{2-}\}}{K_{sp}} \quad (2)$$

where $a\{X\}$ is the ionic activity and K_{sp} is the solubility product for brushite at 37 °C (log $K_{sp} = -6.63$) (Gregory *et al.*, 1970). The activities of all solution species were calculated

using the Davies extended form of the Debye-Hückel equation using mass balance expressions for total calcium and total phosphate with appropriate equilibrium constants by successive approximation for the ionic strength (Table 2).

Table 1: Base growth solutions used for in-situ AFM measurements

Solution	[CaCl] mM	[KDP] mM	pH	IS M	S
1	0.85	60	6	0.15	1.53
2	1.35	5.1	6.5	0.04	1.32
3	8.5	8.5	5.6	0.15	1.56

Table 2: Equilibria used to perform speciation calculation

Equilibria	log k_a	Reference
$H^+ + PO_4^{3-} \Leftrightarrow HPO_4^{2-}$	12.18	(Bjerrum and Unmack, 1929)
$H^+ + HPO_4^{2-} \Leftrightarrow H_2PO_4^-$	7.18	(Bates and Acree, 1943; Bates and Acree, 1945)
$H^+ + H_2PO_4^{2-} \Leftrightarrow H_3PO_{4(aq)}$	2.21	(Bates, 1951)
$Na^+ + HPO_4^{2-} \Leftrightarrow NaHPO_4^-$	1.11	(Smith and Alberty, 1956)
$K^+ + HPO_4^{2-} \Leftrightarrow KHPO_4^-$	1.00	(Smith and Alberty,

		1956)
$\text{Ca}^+ + \text{PO}_4^{2-} \Leftrightarrow \text{CaPO}_4^-$	6.15	(Zhang <i>et al.</i> , 1991)
$\text{Ca}^+ + \text{HPO}_4^{2-} \Leftrightarrow \text{CaHPO}_{4(\text{aq})}$	2.77	(Zhang <i>et al.</i> , 1991)
$\text{Ca}^+ + \text{H}_2\text{PO}_4^{2-} \Leftrightarrow \text{CaH}_2\text{PO}_4^+$	1.45	(Zhang <i>et al.</i> , 1991)

Several strategies were used to prepare growth solutions with various supersaturations or with additives. To measure kinetic coefficients a titration technique was used to vary the supersaturation by increasing the calcium concentration using either base growth solution 1 or 2 (Table 1). A similar technique was also used to investigate etidronate additives. Etidronate is known to complex with calcium, however the micromolar quantities (compared to mM Ca) were too small to substantially effect the supersaturation. It is also known that citrate and oxalate complex with Ca^{2+} and can act to lower the supersaturation for brushite when the concentrations are comparable to that of Ca. For these titration experiments, both CaCl_2 and potassium oxalate or sodium citrate were titrated simultaneously to keep the supersaturation constant. Finally, magnesium is known to lower the supersaturation of brushite by forming complexes with HPO_4^{2-} and for these experiments individual solutions with different magnesium concentrations were prepared keeping the supersaturation constant. All additive experiments used base growth solution 1 except for those with etidronate and one set of citrate data, which used base growth solution 3.

Results and Discussion

Step and surface structure

Brushite crystallizes in a noncentrosymmetric monoclinic structure. Curry and Jones (Curry and Jones, 1971) identified the structure as space group Ia with lattice parameters

$a = 5.812 \text{ \AA}$, $b = 15.18 \text{ \AA}$, $c = 6.239 \text{ \AA}$, and $\beta = 116.25^\circ$. The Ia space group can also be described in an Aa or Cc setting and all three can be related by the use of transformation matrices found in the International Tables of Crystallography. While most experimental work is presented in class Ia, the Ia classification is not recognized in the standard tables and thus more recent papers instead use Aa and Cc. We use Cc to describe our EBSD results.

Brushite has a plate-like morphology dominated by $\{010\}$ faces. (Legeros and Legeros, 1971) The structure (Fig. 1b,c) within the $\{010\}$ plane is composed of two corrugated rows of Ca^{2+} (light blue balls) and HPO_4^{2-} (grey tetrahedrons) that are offset in the $\langle 010 \rangle$ direction. Between these calcium and phosphate containing sheets, are layers of water molecules bound to the calcium ions above and below the $\{010\}$ plane. The weaker bonding of the water molecules to one another creates a cleavage plane between the two water layers perpendicular to the $\{010\}$ face. For this reason the $\{010\}$ faces are fully hydrated even within the bulk structure.

Triangular etch pits and growth hillocks form on the $\{010\}$ faces. Due to the chiral nature of this crystal, the (010) and (0-10) faces have unique steps and therefore the triangular etch pits (or growth hillocks) are mirror images of one another on each face. The etch pits shown in Fig. 2a were formed by etching in DI water inside the AFM fluid cell and the images were acquired in fluid but without fluid flow once the etch pits had stabilized (no measurable step motion). The step edge orientations were measured from AFM images by determining the angle the step makes with the image horizontal. Micrographs were obtained of the crystal's orientation in the AFM and the SEM. These micrographs were used to compare the alignment in both systems and the angle between the edge of the crystal in the two micrographs differed by only 0.25° .

The Euler angles obtained from the EBSD were used to calculate the actual orientation of the crystal normal and step edges of the etch pits. We were able to unambiguously determine the surface orientation as (010), rather than (0-10), and assign the step directions on the as $[10-1]_{\text{Cc}}$, $[101]_{\text{Cc}}$ and $[-100]_{\text{Cc}}$. These values are also related to the Ia setting in Table 3 and shown in relation to the brushite structure in Figure 2b. All SPM images are oriented as shown in Figure 2b.

Table 3. Correlation between the step directions (from EBSD) and primary facets in two crystallographic classes used in the literature. Opposite signs are needed for both facets and steps to describe the $(0 \bar{1} 0)$ face.

Step ^a [UVW]	Face ^b (hkl)	Step [UVW]	Face (hkl)
Cc		Ia	
	(010)		(010)
[-100]	(02-1)	[101]	(-121)
[10-1]	(111)	[-20-1]	(11-2)
[101]	(-111)	[00-1]	(110)

- a The step direction is defined as the cross product between the (010) face and the riser facet and thus is a vector lying within the (010) plane parallel to the step (rather than perpendicular to it). The direction of the step (advancing versus retreating) is made unique by choosing the (hkl) of the riser to point in the direction of the step motion.
- b The facets are given in the direction of step motion for hillocks growing on a (010) facet and are assumed to create an angle that is obtuse with respect to the underlying plane as is suggested by macroscopic crystal habit.

The crystallographic orientations obtained in this work by EBSD agree with those previously reported using other atomic-resolution SPM (Scudiero *et al.*, 1999; Kanzaki *et al.*, 2002) and SEM (Ohta *et al.*, 1979) for identification. While these techniques provided the correct assignments they are more open to interpretation than EBSD. For example, atomic resolution SPM is subject to surface cleanliness, tip sharpness, and scanning conditions. And, the previous SEM work was based upon comparisons between macroscopic morphology and etch pit shape. Given the considerable variation in brushite crystal habit, this requires assumptions regarding bounding facets. Performing EBSD in an SEM has several advantages. No special sample preparation is required and SEM micrographs can be directly compared with morphological features from another imaging techniques. Most importantly, the diffraction method provides an unambiguous assignment of the crystallographic features of interest.

There are several features of the atomic structure that can play a role in crystallization dynamics. Within the crystal, each calcium ion is bonded to 8 oxygen atoms (Figure 2), six from neighboring phosphates (in red) and two from water molecules (in dark blue). Thus, at a step edge, where oxygen atoms are not available from neighboring phosphates, it is likely that the calcium ion will complete its coordination by binding water or OH⁻ groups from the solution. As a reminder that unfulfilled oxygen bonds exist on these edges, the step-edges displayed in Figure 2b are cut such that the CaO₈ coordination (Figure 2c) remains intact. However, it should be noted that the exact form of the hydrated step edge is unknown. As the crystal grows, the oxygen atoms from the solution will need to be removed (or rearranged) to accommodate the adsorbing HPO₄²⁻ ion and thus dehydration is expected to be an important part of the activation barrier for growth and dissolution (Vandervoort and Hartman, 1991). But, because, two water molecules remain as part of the crystal structure, this effect may be expected to be smaller than for unhydrated crystals such as HAP and calcite.

It is also interesting that the {010} faces are fully hydrated as part of the bulk crystal structure and thus the removal of tightly bound water at an {010} surface is not a part of the activation barrier on this facet. In other words, the large surface area of this facet is due to low surface energy rather than to kinetic barriers associated with dehydration. And, in fact, brushite has a relatively low interfacial energy of 4.5mJ/m² (Tang *et al.*, 2005) compared to other biominerals such as 8mJ/m² for apatite (Nancollas 2006) or 13.1mJ/m² for COM (Wu and Nancollas, 1999). SXRD studies show that this water layer is crystalline, but not ice-like and does not impart order of water molecules into the solution as might be expected from ice (Arsic *et al.*, 2004). The fully hydrated surface also suggests that proteins are less likely to bind strongly to these surfaces, as has been observed experimentally (Hanein *et al.*, 1993; Flade *et al.*, 2001). This is likely to play a role in the resorption properties of brushite cements.

Impact of structure on processing

Beyond biocompatibility, two physicochemical properties that lead to brushite's utility are its low surface energy compared to other calcium phosphate phases, and its metastability at physiological pH's. When two minerals compete for common ions, both

the kinetics of formation as well as the relative thermodynamic stability of the two solids play roles in the temporal evolution of the solid-solution mixture. In the case of brushite and apatite, the former has faster formation kinetics and the latter has greater stability.

At physiological pH, apatite is the more thermodynamically stable phase as suggested by the solubility product of 3.47×10^{-9} (Mcdowell *et al.*, 1977) versus 2.34×10^{-7} (Gregory *et al.*, 1970) for brushite. Accordingly, at sufficiently high pH, when PO_4^{3-} is present, apatite will outcompete brushite for calcium and HPO_4^{2-} . However, from classical nucleation theory, the activation barrier associated with homogeneous nucleation from solution (Δg_{nuc}) has a magnitude that depends sensitively on the interfacial energy (γ_{sl}),

$$\Delta g_{nuc} \propto \frac{\gamma_{sl}^3}{\Delta\mu^2} \quad (3)$$

Accordingly, at the same driving force ($\Delta\mu$) the solid with the lower interfacial energy, γ_{sl} , will have the lower nucleation barrier. From the kinetic perspective, brushite crystals will precipitate faster from solution due to their lower interfacial energy of 4.5 mJ/m^2 (Tang 2005) versus 8 mJ/m^2 for apatite (Nancollas *et al.*, 2006).

Step kinetics

Step kinetics reflect the first order rate constants associated with the crystallization reaction $A_{(soln)} \rightarrow A_{(crystal)}$; for this reason, they are fundamental to understanding kinetic controls on crystallization dynamics. Crystallization occurs as Ca^{2+} and HPO_4^{2-} “growth units” (Boistelle and Lopezvalero, 1990) move from the solution phase, overcome an activation barrier, and incorporate into a step at on crystal surface. With this picture in mind, the step velocity (v_s) for a two-component crystal such as brushite, can be written as (Qiu and Orme, 2008; Zhang and Nancollas, 1998)

$$v_s = \beta \sqrt{K_{sp}^\#} \frac{\Omega_{DCPD}}{2} (S^{1/2} - 1) \quad (4)$$

where β is the kinetic coefficient with units of velocity, K_{sp} is the solubility product converted from molar units to number density ($3.87 \times 10^{17} \text{ cm}^{-3}$), $\Omega/2$ is the average volume per growth unit ($6.16 \times 10^{-23} \text{ cm}^3$) and S represents the solubility product defined

by Eq. 2. The kinetic coefficient is related to the first order rate constant (k) and contains the activation barrier associate with adsorption:

$$\beta = \frac{b_{\perp}}{n_k} k^+ = \frac{b_{\perp}}{n_k} v^+ e^{-\Delta\mu/k_B T} \quad (5)$$

where b_{\perp} is the lattice spacing perpendicular to the step, n_k is the number of growth units between kinks, v^+ is the attempt frequency associated with adsorption, and $\Delta\mu$ is the chemical potential difference between the solution and an activated state associated with the barrier. This equation implicitly assumes that the activation barriers associate with Ca^{2+} and HPO_4^{2-} ions are equivalent. A similar formalism is used to describe dissolution except that the relative undersaturation is given by $1-S^{1/2}$.

The relationship between hillock geometry and crystal parameters

At modest supersaturations, brushite grows in the form of triangular hillocks initiating at dislocations. The step directions depend on the underlying crystallography as described above but the density of steps depends on the kinetics and the interfacial energy. Hillock geometry is not available from bulk experiments and is additional information that can be utilized to provide more detailed information on surface interactions. Hillock geometry depends upon the critical length, the step velocities in the different crystallographic directions, and the driving force. Details are provided in (Qiu and Orme, 2008); here, we summarize pieces that are needed to explain data.

Steps emerging from a dislocation do not propagate until they reach a critical length. The critical length is proportional to the step free energy (γ) and the chemical potential:

$$L_c \propto \frac{\gamma}{\Delta\mu} \quad (6)$$

where the chemical potential is $\Delta\mu = kT \ln S$. For each of the three steps, there is a delay before the step reaches the critical length and begins to propagate. Thus, the time it takes to go around the spiral once, one period (T_s) is the sum of these three delay times. From the form of the critical length, it can be seen that the period is proportional to the

interfacial energy and inversely proportional to the driving force. (Note that the critical lengths and velocities differ for each direction. More detailed expressions for L_c and T_s take this into account, however the scaling is as shown).

The density is related to the distance between steps, which is simply the velocity of the step in a given direction (i), multiplied by the spiral period, T_s , or $w_i = v_i T_s$. Accordingly, changes in the critical length lead to changes in the step density. This relation also shows that $w_i \propto v_i$ so that the ratio of terrace widths in the three crystallographic directions is the same as the ratio of velocities, $w_1 : w_2 : w_3 \Leftrightarrow v_1 : v_2 : v_3$.

Dissolution behavior of brushite

The dissolution of brushite has previously been studied by AFM both in solutions without additives (Scudiero *et al.*, 1999; Kanzaki *et al.*, 2002) and in the presence of calcium chelators, such as poly(sodium)aspartate (Peytcheva and Antonietti, 2001). Scudiero *et al.* (1999) discussed dissolution by both chemical and mechanical means. In undersaturated solutions they measured the step velocities of the etch pits and found that the dissolution rate goes as $[-101]_{Cc} > [-10-1]_{Cc}$ while the $[100]_{Cc}$ step had no observable velocity. Note that the step directions have opposite signs from those shown in figure 2 to describe etch pits rather than growth hillocks on the (010) face.) Kanzaki *et al.* (2002) measured the step kinetics over a range of undersaturations and extracted a kinetic coefficient of, $\beta_{[-10-1]_{Cc}} = 0.007$ cm/s. (Their reported value was recalculated to reflect Eq. 4). This value is two orders of magnitude smaller than that found for growth. At this point, it is not yet known whether the difference between kinetic coefficients for growth and dissolution is a materials property or whether it reflects differences in the solution environment.

Growth behavior of brushite without additives

To obtain the kinetic coefficient for growth, step velocity was measured as a function of the relative supersaturation (Figure 3). Experiments were performed using calcium titration to increase the supersaturation, starting from two different base solutions: one with an order of magnitude higher phosphate concentration (closed circles) than the other (open circles). First, the velocity are linear with respect to the

relative supersaturation as predicted by Eq. 4, and fit well even when constrained to go through the origin. However, it is also clear that step kinetics in solutions with more phosphate are faster than those with lower phosphate, even when the relative supersaturation ratio is the same. This implies that the activation barrier for Ca^{2+} and HPO_4^{2-} ions differ. As a result, the crystallization kinetics depend explicitly on the $\{\text{HPO}_4^{2-}\}/\{\text{Ca}^{2+}\}$ ratio, not just the product as is assumed by Eq. 4. These data are complicated by the fact that the pH and ionic strength are also different for the two sets of data. However, a more controlled set of experiments performed at constant supersaturation, constant pH, constant ionic strength, and spanning over two orders of magnitude in $\{\text{HPO}_4^{2-}\}/\{\text{Ca}^{2+}\}$ ratio (Giocondi *et al.*, 2009) have shown that HPO_4^{2-} incorporation is rate-limiting and that the growth rate can be doubled in solutions with high $\{\text{HPO}_4^{2-}\}$ to $\{\text{Ca}^{2+}\}$ ratios.

Despite variations due to anion to cation ratio, use of Eq 4 gives a kinetic coefficient of 0.26 - 0.3 cm/s. A comparison with calcium carbonate (Teng *et al.*, 1999), and calcium oxalate (Orme and Giocondi, 2007b; Onuma *et al.*, 1996; Teng *et al.*, 1999; Weaver *et al.*, 2007), shows that the kinetic coefficients are within a factor of 3 of one another (Qiu and Orme, 2008). By contrast, the kinetic coefficient for HAP (Onuma *et al.*, 1996) is two orders of magnitude smaller, a value more typical of protein crystallization. These differences are used to argue that calcium carbonate, calcium oxalate, and brushite grow via anion and cation attachment, whereas HAP grows via incorporation of larger clusters of molecules (Onuma, 2006).

For both CDHA and DCPD cement formation, the desired goal is to slow the growth rate of brushite crystallization (Figure 1) to increase the setting time. Step kinetic data have demonstrated that HPO_4^{2-} incorporation is the rate-limiting step in brushite crystallization. If these solution results translate to slurries then, brushite kinetics are expected to be slower, and setting times longer, using mixtures with excess free calcium rather than excess free HPO_4^{2-} . Additionally, although purely as a speculation at this point, if it were possible to tune the growth units from single molecules to larger clusters by using solvents or surfactants, it may be possible to alter kinetic coefficients and hence growth rate.

Step anisotropy

The anisotropic nature of the steps makes it interesting to correlate stable step structure and relative kinetic coefficients with the underlying crystal structure. Both growth and dissolution data report that the $[-100]_{\text{Cc}}$ step has the slowest kinetics (Scudiero *et al.*, 1999; Kanzaki *et al.*, 2002; Tang *et al.*, 2005). There are several features that make this step unique compared to the other two. First, along this step direction the chains of calcium and hydrogen phosphate are bonded at the same level rather than in a corrugated manner as they are in the other two directions. This means that this direction has tight ionic bonding within the step giving it low step specific energy. Scudiero *et al.* point out that the calcium ions within this step have 5 nearest neighbor bonds compared with 4 nearest neighbor bonds for the other steps. Another feature that may play a role in the dynamics (Abbona *et al.*, 1994; Scudiero *et al.*, 1999) of this step, is that the acidic hydrogen atom points into solution at the step edge (Figure, in black). It has been suggested that the OH^- molecules hydrogen bond with water in solution, which must then be removed before the next crystallizing molecule can be adsorbed, leading to higher activation barriers for this step. The complementary $[100]_{\text{Cc}}$ step, which is chemically similar within the plane of the step but does not have an OH^- group extending into solution, is not observed under normal conditions, supporting this idea. Interestingly, oxalate, at sufficiently high concentrations, causes the appearance of this step.

Influence of additives on brushite growth

There are several generic ways that adsorbates can affect growth. They can incorporate into the crystal, they can change kinetic coefficients, they can pin steps, and they can act as surfactants. Each of these alters the step kinetics in characteristic ways that allow the differing mechanisms to be distinguished. The interested reader is referred to recent reviews on this subject for more detail (De Yoreo and Vekilov, 2003; Qiu and Orme, 2008).

The impact of magnesium on brushite growth

Magnesium is the second most abundant divalent cation found in biological fluids such as serum, urine, and saliva. It is found in the carbonated-hydroxyapatite of bones

and teeth and it is known that magnesium impurities inhibit both the nucleation and growth of calcium phosphates. Of interest to biological cements, magnesium can stabilize amorphous calcium phosphate against phase transformation (Termine *et al.*, 1970), promote the formation of whitlockite (Mg-substituted tricalcium phosphate) (Rowles, 1968), and inhibit the transformation of brushite to OCP and HAP (Bigi *et al.*, 1988). Previous studies of the effects of magnesium on the growth of brushite have found that magnesium acts as a growth inhibitor but it also stabilizes brushite against dissolution up to neutral pH (Abbona and Franchini-Angela, 1990; Abbona *et al.*, 1986).

SPM was used to look at the growth of brushite in growth solutions with up to $[\text{Mg}^{2+}]/[\text{Ca}^{2+}] = 3$. These results (figure 4) show that magnesium slows the growth rate of all steps at the highest magnesium concentrations. Specifically, the velocity of the $[10\bar{1}]_{\text{Cc}}$ step initially increases with the addition of magnesium, but then decreases linearly as a function of magnesium to calcium ratio (Fig. 4c). The rate of the $[-100]_{\text{Cc}}$ step is similarly affected while the rate of the polar $[101]_{\text{Cc}}$ is slowed the most. These growth rates are depicted pictorially in Fig. 4d where the dotted line shows the initial step rates and the solid shows the rates with Mg. The changes in relative velocity as the magnesium concentration increased resulted in hillock morphologies that changed from the normal triangular shape to one with a greater proportion $[101]_{\text{Cc}}$ compared to $[10\bar{1}]_{\text{Cc}}$. For this to occur, the $[101]_{\text{Cc}}$ step became more (stepped) giving it an overall curved appearance.

The step density also increased due to Mg. The increased step density likely stems from reduced step free energy due to the adsorption of Mg onto surface steps. This would lead to a smaller critical length and a tighter winding of the spiral (Eq. 6). This is supported by nucleation studies, where it was found that magnesium reduced the weighted average step-edge free energy for brushite from 29 pJ/m in pure solutions to 17 pJ/m in the presence of Mg (Lundager Madsen, 2008).

Additionally, the size of the magnesium ion suggests that it may be able to substitute for calcium in the brushite lattice. In the current experiments, Mg was not detected by energy dispersive spectroscopy (EDS) but a higher sensitivity technique is likely needed for overgrowth experiments. Previous experiments have demonstrated that Mg incorporates into the brushite structure resulting in increased lattice parameters (Lilley *et al.*, 2005) and changes to the metal-phosphate bonds (Kumta *et al.*, 2005). At

lower concentrations Mg incorporates fully with concentrations up to 2.8 atomic % (Kumta *et al.*, 2005). At higher concentrations (~17 atomic %), FTIR and XRD show that the magnesium is not fully incorporated into the structure but is also partially associated with amorphous CaP while the morphology transforms from plates to nano-sized spheres. FTIR also shows that the magnesium that is incorporated into the structure causes lattice strain. This strain may explain fluctuations on the $[-100]_{Cc}$ and polar $[101]_{Cc}$ steps as seen in SPM (Fig. 4b). The regular oscillations appear to be periodic, faceted steps. The morphology on the $[-100]_{Cc}$ step can be contrasted with etidronate (figure 7b), which is more characteristic of random disorder.

The implications for the use of magnesium in cement formulations are two-fold. First, the inhibitory effect that magnesium has on brushite nucleation and growth can extend the setting time. Secondly, magnesium inhibits the hydrolysis of brushite to HAP extending the range of solutions where brushite is stable, also increasing the setting time. It should also be noted that effect of magnesium on the supersaturation of brushite was corrected for in the SPM experiments. Magnesium can also be used to lower the supersaturation of brushite by complexing with HPO_4^{2-} . This complexation would lower the growth rate both by reduced supersaturation and removing the rate-limiting unit (HPO_4^{2-}).

The impact of citrate on brushite growth

It is well established that citrate, a small molecule with three carboxyl groups, has an inhibitory effect on CaP crystallization. This property is used beneficially to reduce kidney stone formation (Breslau *et al.*, 1995), and similarly, to extend the setting time (Bohner *et al.*, 1996; Barralet *et al.*, 2004) and shelf life (Gbureck *et al.*, 2005) of CaP cements. To better understand the mechanisms that underlie this inhibitory action, parallel constant composition and SPM experiments were conducted.

Constant composition experiments showed that citrate, $C_3H_5O(COO)_3^{3-}$, inhibited the bulk growth rate of brushite seeds (Tang *et al.*, 2005). Concentrations of 2.1 μ M and 10 μ M citrate reduced the growth rate by 50% and 95%, respectively. Surprisingly, corresponding SPM experiments showed no reduction in step speed and, in fact, step kinetics increased by a small amount (Figures 5a,b,g and e, lower line). On the other

hand, step density did decrease in the presence of citrate. And, because the bulk growth rate relies on both of these factors, this could be used to reconcile the two experiments. This density effect proved reversible, as solutions were oscillated between pure and citrate-bearing, suggesting that that citrate was not incorporating into the crystal structure causing strain that would be sustained during subsequent growth cycles. Instead, it suggested a surface effect similar to a surfactant.

As described earlier, the step density depends on how much time passes before steps emerging from a dislocation begin to propagate. This time is related to the critical length for step motion and correspondingly the step-edge free energy. When the step-edge free energy is small, critical lengths are small, and dislocation hillocks are tightly wound, with narrow terraces, whereas when step edge free energies increase, a longer time is needed before a step reaches its critical length and terraces are correspondingly wider. Given this insight, the reduction in step density can be interpreted as an increase in step-edge free energy associated with citrate binding at the surface. Tang *et al.* verified this result by using a thin-layer, wicking method to measure the surface energies of brushite powders in the absence and presence of citrate, finding that the interfacial energy increased from 4.5mJ/m² in pure solutions to 8.9mJ/m² at 10 μ M citrate (Tang *et al.*, 2005). A higher interfacial energy is also expected to increase the barrier to nucleation (Eq. 3), leading to a longer induction time, which was also verified experimentally.

Citrate's effect was also examined over a significantly broader range of concentrations (Fig 5c,d,f, and g upper line) more relevant for cements, than the study described above. The base solutions had a higher supersaturation and, for this reason, the baseline step speed (for the [10-1]_{Cc} step) was \sim 16nm/s. Despite substantially higher concentrations of citrate, spanning almost 3 orders of magnitude, and up to a 1:1 citrate to calcium ratio, the velocity of the [10-1]_{Cc} step did not vary (Fig 5e). It is interesting that under these conditions the step density was not observed to decrease as it had at lower citrate to Ca ratios. The primary concentration dependent effect was the steady slowing of the polar [101]_{Cc} step, as the citrate concentration increased. At the highest concentration tested (1 mM), the velocity of the polar step had decreased by a factor of \sim 3. The fact that only one step direction is observed to change, suggests that citrate binds

specifically to the $[101]_{Cc}$ step; it seems likely that the negative carboxyl groups interact with the calcium-terminated polar step.

Overall, the implications for macroscopic crystallization are that brushite crystals are less likely to nucleate in the presence of citrate. This effectively expands the metastable regime delaying the precipitation of crystals. Also, brushite crystallites that do form have significantly slower growth rates either due to lower step density, at low concentrations, or, specific interactions at the polar step, at higher citrate to Ca ratios. Both of these effects would have the beneficial effect of increasing the setting time for cements. Somewhat trivially, chelating, (if it were not explicitly corrected for, as in the experiments above) would also lower the growth rate by changing the supersaturation. And, at sufficiently high concentrations citrate will even cause brushite to dissolve.

The impact of oxalate on brushite growth

It is interesting to compare citrate, which has 3 carboxyl groups, with oxalate, which has two. The kinetics are similar in that neither affects the growth rate of the $[10-1]_{Cc}$ step (figure 6c). But, under the same conditions, citrate interacts with the polar step whereas oxalate does not. Given that citrate and oxalate both have carboxyl moieties, this would suggest that the geometry (stereochemistry) is not well matched between oxalate and the polar step. Instead, oxalate causes a new facet to appear (figure 6b, d). The new facet is the mirror to brushite's most stable $[-100]_{Cc}$ step except that this is the direction that does not present a hydroxyl group at the step edge (in other words, a $[100]_{Cc}$ step as discussed earlier).

The effect of oxalate does not present any advantages to tuning cement processing. But, it does present clues and more stringent tests that may aid modelers in determining how additives interact with brushite surfaces. In addition, because calcium oxalate forms a solid product (as opposed to calcium citrate complexes, which are aqueous) it may have commonalities with brushite to apatite transitions. In the case of calcium oxalate, SPM has shown that the conversion from brushite to COM is a dissolution reprecipitation reaction, where brushite serves as a reservoir of Ca rather than an epitaxial template (Tang *et al.*, 2006). This is similar to what might be anticipated if ACP were the precursor stage. Although no in situ experiments have yet captured the

evolution of brushite to apatite, the brushite to COM transition may serve as a reasonable model to describe this process.

The impact of bisphosphonate on brushite growth

The bisphosphonate, etidronate (ethylene-1-hydroxy-1,1-diphosphonate), has been found to inhibit osteoclast activity and is considered therapeutic in diseases that require the regulation of bone remodeling (such as Pagets's disease, osteoporosis and osteolytic tumors) (Rodan and Martin, 2000). Bisphosphates are structurally similar to pyrophosphate ($P_2O_7^{4-}$) except that the oxygen molecule that joins the two phosphate groups in pyrophosphates is substituted with a more robust carbon atom. This makes them less susceptible to biodegradation, an asset for their therapeutic use. The carbon substitution also has the advantage of adding two more binding sites, allowing a variety of side groups to be added to the molecule (Papapoulos, 2006). Etidronate is a bisphosphonate with a hydroxyl bound to the central carbon. This configuration is thought to allow a tridentate binding to calcium ions (Papapoulos, 2008).

The incorporation of bisphosphonates into cements is under consideration as a drug delivery mechanism (Grover *et al.*, 2006). However, because of their structural similarity to pyrophosphates some of the physicochemical effects observed for pyrophosphate, may also pertain to etidronate. In cements, pyrophosphate has been shown to improve mechanical properties (Grover *et al.*, 2006; Alkhralsat *et al.*, 2008); reduce setting time (Bohner *et al.*, 1996; Rodan and Martin, 2000), and reduce the likelihood of conversion to apatite (Grover *et al.*, 2006).

Although several studies have examined the effect of pyrophosphate on DCPD growth and dissolution few studies discuss the interaction of etidronate with brushite. The only study that we are aware of, (Grases *et al.*, 2000), showed that etidronate inhibited both growth and nucleation more effectively than pyrophosphate.

To investigate this interaction further, SPM was employed to monitor DCPD step kinetics and morphology in the presence of up to $7\mu\text{M}$ etidronate (figure 7). There are two significant findings. The first is that the images clearly show that etidronate interacted with, and inhibited growth on, the polar $[101]_{Cc}$ steps of brushite. In fact, the second, mirror step $[-10-1]_{Cc}$ also became stabilized, changing the normal triangular step

pattern into a four-sided trapezium. The second finding is that while the polar steps became slower, the $[10-1]_{cc}$ step became significantly faster (figure 7c). The step velocity increased from 9nm/s without etidronate to 15nm/s at a concentration of $7\mu\text{M}$, an increase of 67%. Recalling that the ratio of the terrace widths reflects the ratio of velocities (as described earlier), the velocities change from 9.2, 7.7, and 1.5nm/s to 15.1, 3.1, (3.1), and 1.5nm/s in the $[10-1]_{cc}:[101]_{cc}:[-100]_{cc}$ directions, respectively. The new polar step is shown in parenthesis. The relative velocities are depicted schematically in figure 7d, where the dotted triangle represents the case without additive and the solid line reflects the case after etidronate addition. All velocities are referenced with respect to the dislocation origin (black dot).

This data suggests that the negative phosphate and possibly hydroxyl groups preferentially bind to the calcium-terminated polar steps. This is the primary source of etidronate's inhibitory action on DCPD. Etidronate does not appear to bind strongly to the steps with mixed charge; the evidence for this is fact that the velocity of the slow $[00-1]$ step does not change when etidronate is added. The step becomes less straight and well defined, but does not slow. The change in morphology may be evidence of step pinning, but below the threshold necessary to alter the kinetics significantly. The other mixed charge step, $[10-1]_{cc}$, speeds up. Although, etidronate is clearly affecting this step, it is unlikely to be strongly bound, as this would block growth sites, slowing kinetics, as is observed for the polar steps.

The increase in step kinetics due to additives has been observed for a number of other systems (Kim *et al.*, 2006; Elhadj *et al.*, 2006; Fu *et al.*, 2005). In fact, Mg, citrate and oxalate all show some evidence of this at low concentrations, with velocities slightly (but systematically) above the baseline value. There are a number of proposed mechanism including, increasing kink density, increasing surface cation or anion concentrations, and altering activation barriers. It also seems unlikely that etidronate acts as a surface phosphate source first, because the central carbon bond makes it unlikely that etidronate will break apart and second, because effects are seen with concentrations as low as $1\mu\text{M}$ (compared to solution concentrations of HPO_4^{2-} in the mM range). A similar argument holds for calcium that may bind to etidronate and concentrate at the surface. Instead, it seems more reasonable that etidronate alters the water layer near the surface or

acts as a bridge between the solution and the crystal, effectively lowering the barrier for Ca^{2+} or HPO_4^{2-} incorporation.

The change in hillock shape also suggests a change in macroscopic morphology. Macroscopic habit is dominated by the geometry of the growth steps. In the case of brushite, the macroscopic shape reflects the triangular hillocks on the (010) and (0-10) faces, which are mirrors of one another. This is demonstrated schematically in Figure 8a showing long platelets dominated by the $\{02-1\}$ facets (which correspond to the slow $[\langle -100 \rangle]$ steps). When etidronate is added, the macroscopic shape should reflect the new trapezium (figure 8b), which is dominated by the polar $\{-111\}$ facets. By contrast, citrate or Mg, additives are not expected to alter the shape dramatically because the hillock remains approximately triangular even though the proportions change somewhat. Unfortunately, we do not have SEM images to verify this prediction but note, that unless care is taken with identifying the orientation, the etidronate crystal shape can be misconstrued as being similar to normal brushite crystals.

Conclusion and Outlook

In summary, SPM data has shown that (1) Mg inhibits growth on all steps but relatively high Mg/Ca ratios are needed. Extracting the mechanism of interaction requires more modeling of the kinetic data, but step morphology is consistent with incorporation. (2) Citrate has several effects depending on the citrate/Ca ratio. At the lowest concentrations, citrate increases the step free energy without altering the step kinetics; at higher concentrations, the polar step is slowed. (3) Oxalate also slows the polar step but additionally stabilizes a new facet, with a $[100]_{\text{Cc}}$ step. (4) Etidronate has the greatest kinetic impact of the molecules studied. At $7\mu\text{M}$ concentrations, the polar step slows by 60% and a new polar step appears. However, at the same time the $[10-1]_{\text{Cc}}$ increases by 67%. It should be noted that all of these molecules complex calcium and can effect kinetics by altering the solution supersaturation or the Ca to HPO_4^{2-} ratio. For the SPM data shown, this effect was corrected for to distinguish the effect of the molecule at the crystal surface from the effect of the molecule on the solution speciation.

The goal of this paper is to draw connections between fundamental studies of atomic step motion and potential strategies for materials processing. It is not our intent to promote the utility of SPM for investigating processes in cement dynamics. The conditions are spectacularly different in many ways. The data shown in this paper are fairly close to equilibrium ($S=1.6$) whereas the nucleation of cements is initiated at supersaturation ratios in the thousands to millions. Of course, after the initial nucleation phase, the growth will occur at more modest supersaturations and as the cement evolves towards equilibrium certainly some of the growth will occur in regimes such as shown here. In addition to the difference in supersaturation, cements tend to have lower additive to calcium ratios. As an example, the additive to Ca ratio is $\sim 10^{-3}$ to 10^{-4} for a pyrophosphate based cement (Grover *et al.*, 2006).

Where the *in situ* SPM approach provides unique insights is in providing details of where and how molecules inhibit or accelerate kinetics. This has the potential to aid in designing molecules to target specific steps and to guide synergistic combinations of additives. For example, it is unlikely that bulk techniques could deduce the simultaneous acceleration and inhibition effects of etidronate; or that citrate reduced growth rate by altering step density rather than step speed. In addition, SPM data translates to tractable questions for modelers. The questions changes from “How does etidronate inhibit brushite growth?” to “Why does etidronate bind strongly to the $[101]_{Cc}$ step while it doesn't to the $[10-1]_{Cc}$ step?” This is still a challenging question but it is far better defined.

Given that step chemistries are generally different, it seems reasonable to expect that the greatest inhibition will be achieved not with one, but with several synergistically chosen additives. For example, the most effective growth inhibitors for brushite would target the two fast steps, namely the non-polar, $[10-1]_{Cc}$ and the polar, $[101]_{Cc}$ steps. Several molecules have been shown to slow the polar step, with etidronate as the most dramatic example. By contrast, only Mg was observed to slow the $[10-1]_{Cc}$ step. Thus, a combination of high concentrations of Mg to target the $[10-1]_{Cc}$ step with low concentrations of etidronate to target the polar steps, should be a more effective combination than either alone. However Mg is not a particularly good inhibitor in the sense that high concentrations are needed, and it is not specific. More ideally, an inhibitor

would be designed to interact specifically with the [10-1] step, which would allow the two steps to be independently modified. Again, this provides an opportunity for tighter coupling with theoretical modeling. The question changes from “What types of molecules will inhibit brushite growth” to “What type of molecule will interact with the [10-1]_{Cc} step?” Similarly, to increase resorption rate, it would be most efficacious to target the slow moving [-100] step, perhaps by targeting the hydroxyl group which seem to stabilize this step compared to its otherwise similar mirror, [100].

In short, there are a number of opportunities where molecular scale imaging can provide new information that has the prospect to aid in optimizing calcium phosphate cements.

Acknowledgements

This work was performed under the auspices of the U.S. Department of Energy by Lawrence Livermore National Laboratory under Contract DE-AC52-07NA27344. Portions of this work were supported by the National Institutes of Health (NIDCR DE03223).

Tables

Table 1: Base growth solutions used for in-situ AFM measurements

Solution	[CaCl] mM	[KDP] mM	pH	IS M	S
1	0.85	60	6	0.15	1.53
2	1.35	5.1	6.5	0.04	1.32
3	8.5	8.5	5.6	0.15	1.56

Table 2: Equilibria used to perform speciation calculation

Equilibria	log k_a	Reference
$H^+ + PO_4^{3-} \Leftrightarrow HPO_4^{2-}$	12.18	(Bjerrum and Unmack, 1929)
$H^+ + HPO_4^{2-} \Leftrightarrow H_2PO_4^-$	7.18	(Bates and Acree, 1943; Bates and Acree, 1945)
$H^+ + H_2PO_4^{2-} \Leftrightarrow H_3PO_{4(aq)}$	2.21	(Bates, 1951)
$Na^+ + HPO_4^{2-} \Leftrightarrow NaHPO_4^-$	1.11	(Smith and Alberty, 1956)
$K^+ + HPO_4^{2-} \Leftrightarrow KHPO_4^-$	1.00	(Smith and Alberty, 1956)
$Ca^+ + PO_4^{2-} \Leftrightarrow CaPO_4^-$	6.15	(Zhang <i>et al.</i> , 1991)
$Ca^+ + HPO_4^{2-} \Leftrightarrow CaHPO_{4(aq)}$	2.77	(Zhang <i>et al.</i> , 1991)
$Ca^+ + H_2PO_4^{2-} \Leftrightarrow CaH_2PO_4^+$	1.45	(Zhang <i>et al.</i> , 1991)

Table 3. Correlation between the step directions (from EBSD) and primary facets in two crystallographic classes used in the literature. Opposite signs are needed for both facets and steps to describe the $(0 \bar{1} 0)$ face.

Step ^a	Face ^b	Step	Face
[UVW]	(hkl)	[UVW]	(hkl)
Cc		Ia	
	(010)		(010)
[-100]	(02-1)	[101]	(-121)
[10-1]	(111)	[-20-1]	(11-2)
[101]	(-111)	[00-1]	(110)

- a The step direction is defined as the cross product between the (010) face and the riser facet and thus is a vector lying within the (010) plane parallel to the step (rather than perpendicular to it). The direction of the step (advancing versus retreating) is made unique by choosing the (hkl) of the riser to point in the direction of the step motion.
- b The facets are given in the direction of step motion for hillocks growing on a (010) facet and are assumed to create an angle that is obtuse with respect to the underlying plane as is suggested by macroscopic crystal habit.

Figure captions

Figure 1. Goals and strategies for tuning brushite crystallization kinetics to improve, or better understand, calcium phosphate cement formation. A, B, and C represent various calcium phosphate phase, DCPD represents brushite, and CDHA represents calcium deficient hydroxylapatite.

Figure 2. Brushite etch experiment and structure. (a) SPM micrograph of etch pits on the brushite surface. The inset shows the EBSD diffraction pattern. (b) Crystallographic model of a brushite (010) growth surface with step assignments for space group Cc. Note that the growth geometry is the mirror image of the etch geometry. (c) HPO_4 and Ca-O- H_2O clusters shown in the same orientation as (b). P = grey, O = red, H (HPO_4) = black, Ca = light blue, O (H_2O) = dark blue, H (H_2O) = pink. All SPM images are oriented as indicated in b.

Figure 3. Plots of the velocity of the $[10\text{-}1]_{\text{Cc}}$ step as a function relative supersaturation ($S^{1/2}-1$). Solid points stem from a base solution with an order of magnitude greater phosphate concentration (0.85mM CaCl_2 , 60mM KDP, pH=6, and IS=0.15M) than the points plotted with open circles (1.3mM CaCl_2 , 5.1mM KDP, pH=6.5 and IS=0.04M). The supersaturation was increased by adding 0.1mM and 0.05 mM aliquots of CaCl_2 , respectively.

Figure 4. SPM experiment to determine the effect of Mg^{2+} additives on brushite growth. SPM micrographs of brushite growth in a (a) pure growth solution and (b) with Mg^{2+} . Both images are $2\mu\text{m} \times 2\mu\text{m}$. (c) Plot of the velocity of the $[10\text{-}1]_{\text{Cc}}$ step as a function of $[\text{Mg}^{2+}]/[\text{Ca}^{2+}]$. (d) Schematic drawing comparing the relative step growth kinetics in a pure solution (dashed line) to those with magnesium additives (solid line). The dislocation source is denoted by the dot.

Figure 5. SPM experiments to determine the effect of citrate additives on brushite growth. SPM micrographs of brushite growth in the absence (a,c) and presence (b,d) of citrate. All images are $2\mu\text{m} \times 2\mu\text{m}$. (e) Plots of the velocity of the $[10-1]_{\text{Cc}}$ step as a function of $[\text{citrate}]/[\text{Ca}^{2+}]$. The bottom data set corresponds to the SPM experiment in (a,b) at low citrate concentrations while the top data set corresponds to the SPM experiment in (c,d) at higher citrate concentrations. (f,g) Schematic drawing comparing the relative step growth kinetics in a pure solution (dashed line) to those with citrate additives (solid line at higher and low concentrations, respectively). The dislocation source is denoted by the dot.

Figure 6. SPM experiment to determine the effect of oxalate additives on brushite growth. SPM micrographs of brushite growth in the absence (a) and presence (b) of oxalate showing the emergence of a new step direction. Both images are $2\mu\text{m} \times 2\mu\text{m}$. (c) Plot of the velocity of the $[10-1]_{\text{Cc}}$ step as a function of $[\text{oxalate}]/[\text{Ca}^{2+}]$. (d) Schematic drawing comparing the relative step growth kinetics in a pure solution (dashed line) to those with oxalate additives (solid line). The dislocation source is denoted by the dot.

Figure 7. SPM experiment to determine the effect of etidronate additives on brushite growth. SPM micrographs of brushite growth in a (a) pure growth solution and (b) with etidronate showing the emergence of a new step direction. Both images are $2\mu\text{m} \times 2\mu\text{m}$. (c) Plot of the velocity of the $[10-1]_{\text{Cc}}$ step as a function of $[\text{etidronate}]/[\text{Ca}^{2+}]$. (d) Schematic drawing comparing the relative step growth kinetics in a pure solution (dashed line) to those with etidronate additives (solid line). The dislocation source is denoted by the dot.

Figure 8. Macroscopic habits predicted from hillock geometry (a) in the absence of additives, (b) in the presence of etidronate, and (c) the presence of citrate or Mg. The facets associated with hillock step directions are indicated (see Table 3).

References

- Abbona, F., Calleri, M., Franchiniangela, M. & Ivaldi, G. 1994 Synthetic Brushite, $\text{Ca}_2\text{H}_2\text{O}_7$ - Correct Polarity and Surface-Features of Some Complementary Forms. *Neues Jb Miner Abh*, 168, 171-184.
- Abbona, F. & Franchini-Angela, M. 1990 Crystallization of Calcium and Magnesium Phosphates from Solutions of Low Concentration. *J Cryst Growth*, 104, 661-671.
- Abbona, F., Lundager Madsen, H. E. & Boistelle, R. 1986 The Initial Phases of Calcium and Magnesium Phosphates Precipitated from Solutions of High to Medium Concentrations. *J Cryst Growth*, 74, 581-590.
- Alkhralsat, M. H., Marino, F. T., Other, Other & Other 2008 Combined effect of strontium and pyrophosphate on the properties of brushite cements. *Acta Biomater*, 4, 664-670.
- Arsic, J., Kaminski, D., Poodt, P. & Vlieg, E. 2004 Liquid ordering at the Brushite-{010}-water interface. *Physical Review B*, 69, 4.
- Barralet, J. E., Grover, L. M., 1, O., 2, O. & 3, O. 2004 Ionic modification of calcium phosphate cement viscosity. Part II: hypodermic injection and strength improvement of brushite cement. *Biomaterials*, 25, 2197-2203.
- Bates, R. G. 1951 1st Dissociation Constant of Phosphoric Acid from 0-Degrees-C to 60-Degrees-C - Limitations of the Electromotive Force Method for Moderately Strong Acids. *J Res Nat Bur Stand*, 47, 127-134.
- Bates, R. G. & Acree, S. F. 1943 H values of certain phosphate-chloride mixtures, and the second dissociation constant of phosphoric acid from 0 degrees to 60 degrees C. *J Res Nat Bur Stand*, 30, 129-155.
- Bates, R. G. & Acree, S. F. 1945 Ph of Aqueous Mixtures of Potassium Dihydrogen Phosphate and Disodium Hydrogen Phosphate at 0-Degrees to 60-Degrees-C. *J Res Nat Bur Stand*, 34, 373-394.
- Bigi, A., Gazzano, M., Ripamonti, A. & Roveri, N. 1988 Effect of Foreign Ions on the Conversion of Brushite and Octacalcium Phosphate into Hydroxyapatite. *J Inorg Biochem*, 32, 251-257.
- Bjerrum, N. & Unmack, A. 1929 *Kgl Danske Videnskabernes Selskab Mat-fys Medd* 1, 9.
- Bohner, M. 2007 Reactivity of calcium phosphate cements. *J Mater Chem*, 17, 3980-3986.
- Bohner, M., Lemaitre, J., 1, O., 2, O. & 3, O. 1996 Effects of sulfate, pyrophosphate, and citrate ions on the physicochemical properties of cements made of beta-tricalcium phosphate-phosphoric acid-water mixtures. *J Am Ceram Soc*, 79, 1427-1434.
- Boistelle, R. & Lopezvalero, I. 1990 Growth Units and Nucleation - the Case of Calcium Phosphates. *J Cryst Growth*, 102, 609-617.
- Breslau, N. A., Padalino, P. & Al., E. 1995 Physicochemical Effects of a New Slow-Release Potassium Phosphate Preparation (Urophos-K) Asterisk in Absorptive Hypercalciuria. *J Bone Miner Res*, 10, 394-400.

- Curry, N. A. & Jones, D. W. 1971 Crystal Structure of Brushite, Calcium Hydrogen Orthophosphate Dihydrate - Neutron-Diffraction Investigation. *J Chem Soc A*, 3725-&.
- De Yoreo, J. J. & Vekilov, P. G. 2003 Principles of crystal nucleation and growth. *Rev. Mineral. Geochem.*, 54, 57-93.
- Dorozhkin, S. V. 2008 Calcium orthophosphate cements for biomedical application. *J Mater Sci*, 43, 3028-3057.
- Elhadj, S., De Yoreo, J. J., Hoyer, J. R. & Dove, P. M. 2006 Role of molecular charge and hydrophilicity in regulating the kinetics of crystal growth. *P Natl Acad Sci USA*, 103, 19237-19242.
- Flade, K., Lau, C., Mertig, M. & Pompe, W. 2001 Osteocalcin-controlled dissolution-precipitation of calcium phosphate under biomimetic conditions. *Chem Mater*, 13, 3596-3602.
- Fu, G., Qiu, S. R., Orme, C. A., Morse, D. E. & De Yoreo, J. J. 2005 Acceleration of calcite kinetics by abalone nacre proteins. *Adv Mater*, 17, 2678-2683.
- Gbureck, U., Dembski, S., Other, Other & Other 2005 Factors influencing calcium phosphate cement shelf-life. *Biomaterials*, 26, 3691-3697.
- Giocondi, J. L., Nancollas, G. H. & Orme, C. A. (2009) Does calcium or phosphate limit the growth of brushite?
- Grases, F., Ramis, M. & Costa-Bauza, A. 2000 Effects of phytate and pyrophosphate on brushite and hydroxyapatite crystallization - Comparison with the action of other polyphosphates. *Urol Res*, 28, 136-140.
- Gregory, T. M., Moreno, E. C. & Brown, W. E. 1970 Solubility of $\text{CaHPO}_4 \cdot 2\text{H}_2\text{O}$ in the system of $\text{Ca}(\text{OH})_2\text{-H}_3\text{PO}_4\text{-H}_2\text{O}$ at 5, 15, 25, and 37°C. *J. Res. Natl. Bur. Stds.*, 74a, 461.
- Grover, L. M., Gbureck, U., Wright, A. J., Tremayne, M. & Barralet, J. E. 2006 Biologically mediated resorption of brushite cement in vitro. *Biomaterials*, 27, 2178-2185.
- Hanein, D., Geiger, B. & Addadi, L. 1993 Fibronectin Adsorption to Surfaces of Hydrated Crystals - an Analysis of the Importance of Bound Water in Protein Substrate Interactions. *Langmuir*, 9, 1058-1065.
- Kanzaki, N., Onuma, K., Treboux, G. & Ito, A. 2002 Dissolution kinetics of dicalcium phosphate dihydrate under pseudophysiological conditions. *J Cryst Growth*, 235, 465-470.
- Kim, I. W., Darragh, M. R., Orme, C. & Evans, J. S. 2006 Molecular "tuning" of crystal growth by nacre-associated polypeptides. *Cryst Growth Des*, 6, 5-10.
- Kumta, P. N., Sfeir, C., Lee, D.-H., Olton, D. & Choi, D. 2005 Nanostructured Calcium Phosphates for Biomedical Applications: Novel Synthesis and Characterization. *Acta Biomater*, 1, 65-83.
- Legeros, R. Z. & Legeros, J. P. 1971 Brushite Crystals Grown by Diffusion in Silica-Gel and in Solution. *Journal of Crystal Growth*, 13, 476-&.
- Lilley, K. J., Gbureck, U., Knowles, J. C., Farrar, D. F. & Barralet, J. E. 2005 Cement from magnesium substituted hydroxyapatite. *J Mater Sci-Mater M*, 16, 455-460.
- Lundager Madsen, H. E. 2008 Influence of Foreign Metal Ions on Crystal Growth and Morphology of Brushite ($\text{CaHPO}_4 \cdot 2\text{H}_2\text{O}$) and its Transformation to Octocalcium Phosphate and Apatite. *J Cryst Growth*, 310, 2602-2612.

- Mcdowell, H., Gregory, T. M. & Brown, W. E. 1977 Solubility of $\text{Ca}_5(\text{PO}_4)_3\text{OH}$ in System $\text{Ca}(\text{OH})_2\text{-H}_3\text{PO}_4\text{-H}_2\text{O}$ at 5-Degrees-C, 15-Degrees-C, 25-Degrees-C and 37-Degrees-C. *J Res Nbs a Phys Ch*, 81, 273-281.
- Nancollas, G. H., Tang, R., Phipps, R. J., Henneman, Z., Gulde, S., Wu, W., Mangood, A., Russell, R. G. G. & Ebetino, F. H. 2006 Novel insights into actions of bisphosphonates on bone: Differences in interactions with hydroxyapatite. *Bone*, 38, 617-627.
- Ohta, M., Tsutsumi, M. & Ueno, S. 1979 Observations of Etch Pits on as-Grown Faces of Brushite Crystals. *J Cryst Growth*, 47, 135-136.
- Onuma, K. 2006 Recent research on pseudobiological hydroxyapatite crystal growth and phase transition mechanisms. *Prog Cryst Growth Ch*, 52, 223-245.
- Onuma, K., Ito, A. & Tateishi, T. 1996 Investigation of a growth unit of hydroxyapatite crystal from the measurements of step kinetics. *Journal of Crystal Growth*, 167, 773-776.
- Orme, C. A. & Giocondi, J. L. (2007a) Model Systems for Formation and Dissolution of Calcium Phosphate Minerals. IN BAEUERLEIN, E. & BEHRENS, P. (Eds.) *Handbook of Biomineralization*. Weinheim, Wiley-VCH.
- Orme, C. A. & Giocondi, J. L. (2007b) The Use of Scanning Probe Microscopy to Investigate Crystal-fluid Interfaces. IN SKOWRONSKI, M., DEYOREO, J. J. & WANG, C. A. (Eds.) *Perspectives on Inorganic, Organic, and Biological Crystal Growth*. Melville, AIP Conference Proceedings.
- Papapoulos, S. E. 2006 Bisphosphonate actions: Physical chemistry revisited. *Bone*, 38, 613-616.
- Papapoulos, S. E. 2008 Bisphosphonates: how do they work? *Best Practice & Research Clinical Endocrinology & Metabolism*, 22, 831-847.
- Peytcheva, A. & Antonietti, M. 2001 "Carving on the nanoscale": Polymers for the site-specific dissolution of calcium phosphate. *Angew Chem Int Edit*, 40, 3380-3383.
- Qiu, S. R. & Orme, C. A. 2008 Dynamics of Biomineral Formation at the Near-Molecular Level. *Chem Rev*, 108, 4784-4822.
- Qiu, S. R., Wierzbicki, A., Salter, E. A., Zepeda, S., Orme, C. A., Hoyer, J. R., Nancollas, G. H., Cody, A. M. & De Yoreo, J. J. 2005 Modulation of calcium oxalate monohydrate crystallization by citrate through selective binding to atomic steps. *J Am Chem Soc*, 127, 9036-9044.
- Rodan, G. A. & Martin, T. J. 2000 Therapeutic Approaches to Bone Diseases. *Science*, 289, 1508-1514.
- Rowles, S. L. 1968 *B Soc Chim Fr*, 1797.
- Scudiero, L., Langford, S. C. & Dickinson, J. T. 1999 Scanning force microscope observations of corrosive wear on single-crystal brushite (CaHPO_4 center dot $2\text{H}_2\text{O}$) in aqueous solution. *Tribol Lett*, 6, 41-55.
- Smith, R. M. & Alberty, R. A. 1956 The Apparent Stability Constants of Ionic Complexes of Various Adenosine Phosphates with Monovalent Cations. *J Phys Chem-U.S.*, 60, 180-184.
- Tang, R., Nancollas, G. H., Giocondi, J. L., Hoyer, J. R. & Orme, C. A. 2006 Dual roles of brushite crystals in calcium oxalate crystallization provide physicochemical mechanisms underlying renal stone formation. *Kidney Int*, 70, 71-78.

- Tang, R. K., Darragh, M., Orme, C. A., Guan, X. Y., Hoyer, J. R. & Nancollas, G. H. 2005 Control of biomineralization dynamics by interfacial energies. *Angew Chem Int Edit*, 44, 3698-3702.
- Tang, R. K., Nancollas, G. H. & Orme, C. A. 2001 Mechanism of dissolution of sparingly soluble electrolytes. *J Am Chem Soc*, 123, 5437-5443.
- Tang, R. K., Orme, C. A. & Nancollas, G. H. 2003 A new understanding of demineralization: The dynamics of brushite dissolution. *J Phys Chem B*, 107, 10653-10657.
- Teng, H. H., Dove, P. M. & Deyoreo, J. J. 1999 Reversed calcite morphologies induced by microscopic growth kinetics: Insight into biomineralization. *Geochimica et Cosmochimica Acta*, 63, 2507-2512.
- Termine, J. D., Rechauskas, R. A. & Posner, A. S. 1970 *Arch. Biochem. Biophys*, 140, 318.
- Vandervoort, E. & Hartman, P. 1991 The Habit of Gypsum and Solvent Interaction. *Journal of Crystal Growth*, 112, 445-450.
- Weaver, M. L., Qiu, S. R., Hoyer, J. R., Casey, W. H., Nancollas, G. H. & De Yoreo, J. J. 2007 Inhibition of calcium oxalate monohydrate growth by citrate and the effect of the background electrolyte. *Journal of Crystal Growth*, 306, 135-145.
- Wu, W. J. & Nancollas, G. H. 1999 Determination of interfacial tension from crystallization and dissolution data: a comparison with other methods. *Advances in Colloid and Interface Science*, 79, 229-279.
- Zhang, J. W., Ebrahimpour, A. & Nancollas, G. H. 1991 Ion Association in Calcium-Phosphate Solutions at 37-Degrees-C. *J Solution Chem*, 20, 455-465.
- Zhang, J. W. & Nancollas, G. H. 1998 Kink density and rate of step movement during growth and dissolution of an AB crystal in a nonstoichiometric solution. *J Colloid Interf Sci*, 200, 131-145.

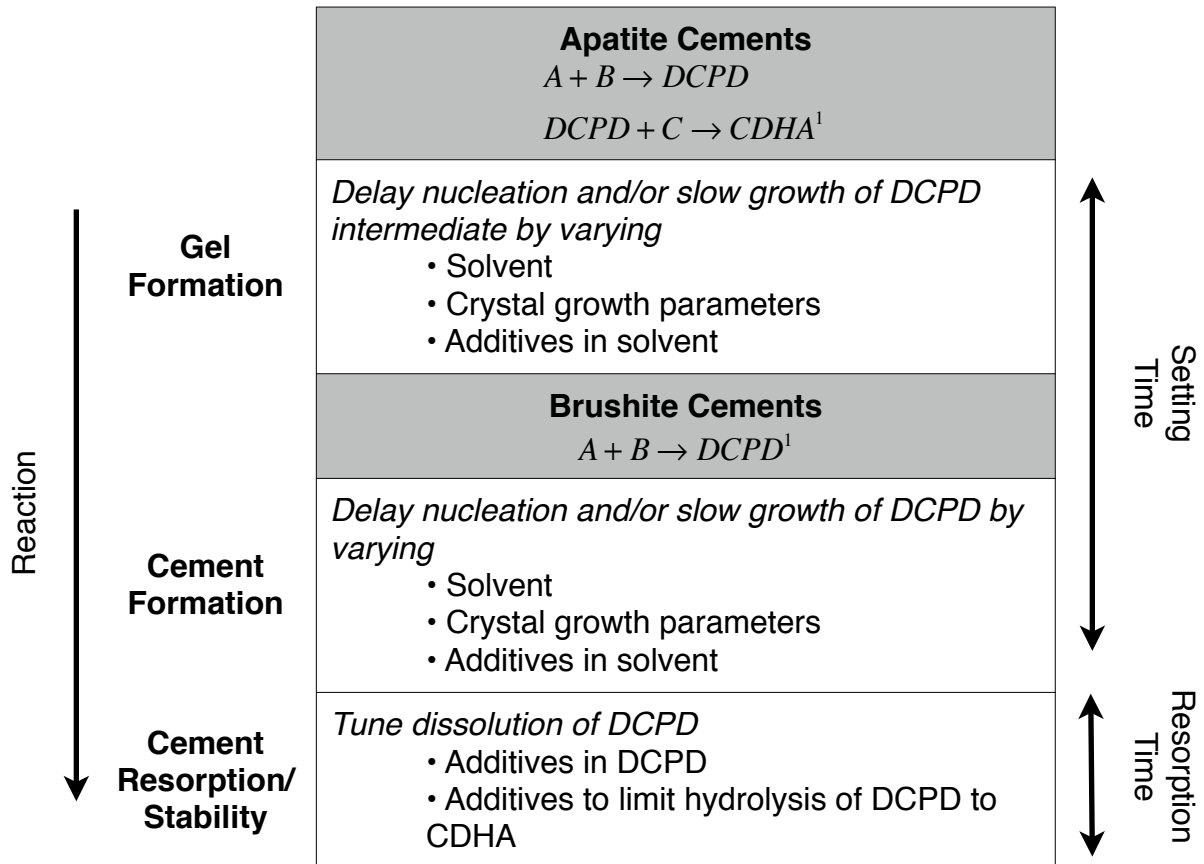


Figure 1

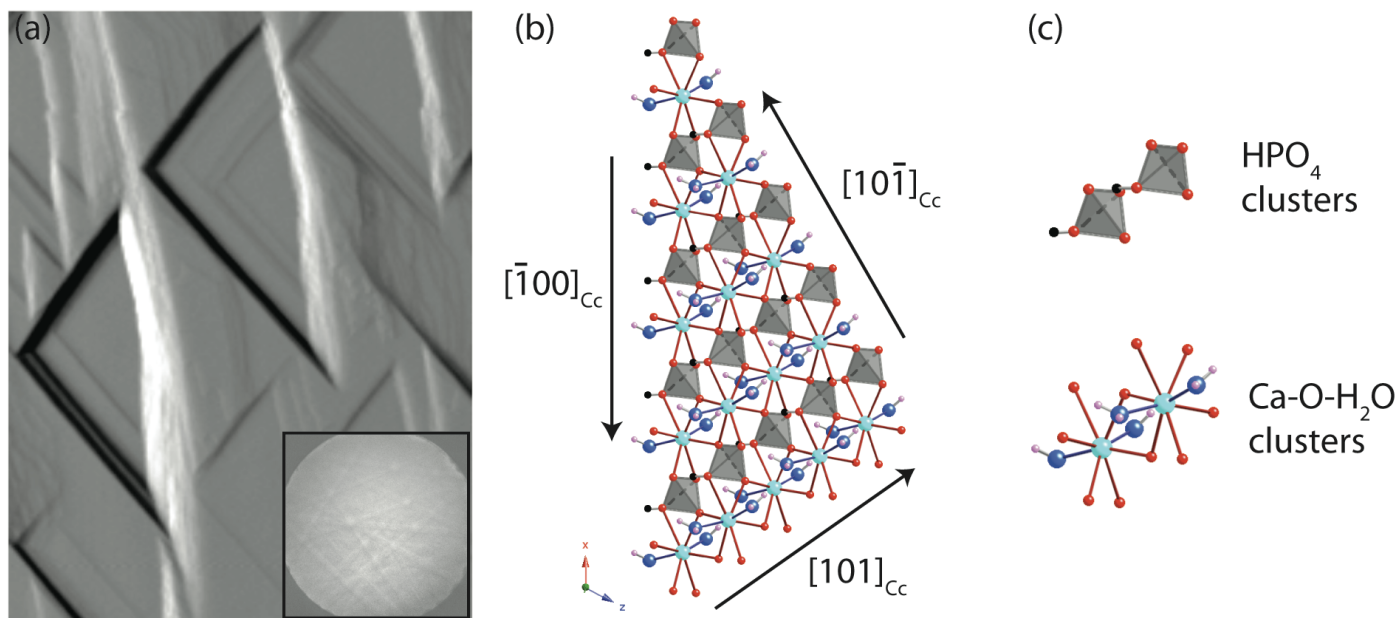


Figure 2. Structure of DCPD

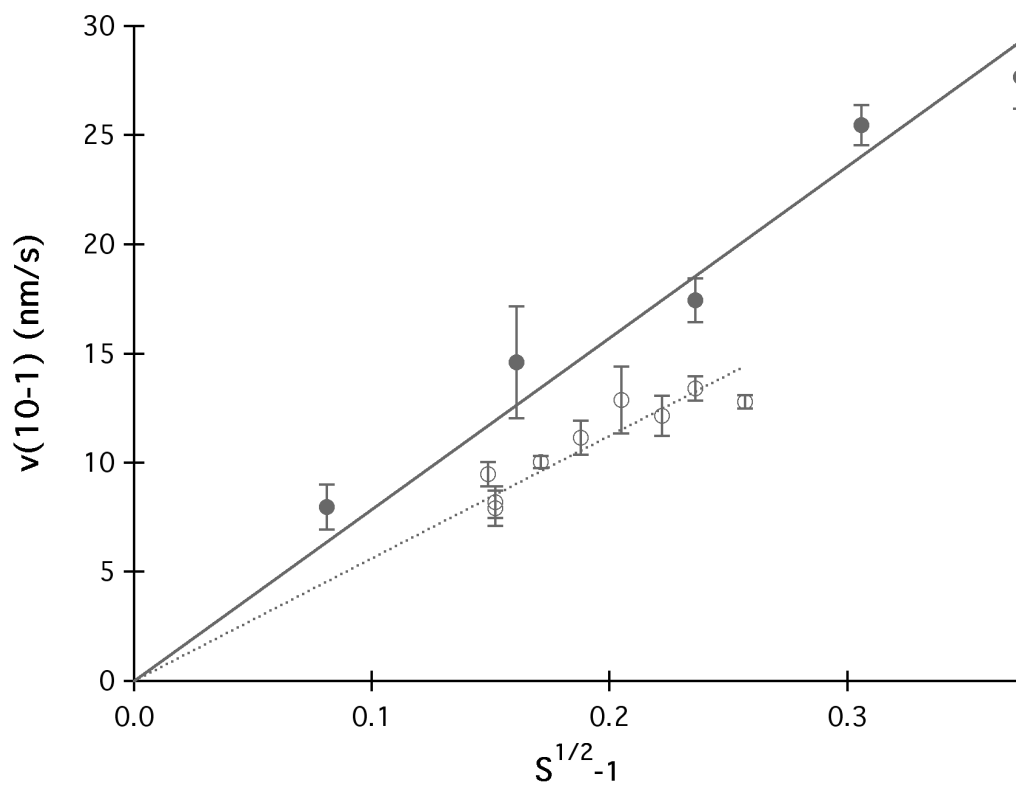


Figure 3. Velocity of the [10-1] step as a function relative supersaturation ($S^{1/2}-1$). Solid points stem from a base solution with an order of magnitude greater phosphate concentration (0.85mM CaCl_2 , 60mM KDP, pH=6, and IS=0.15M) than the points plotted with open circles (1.3mM CaCl_2 , 5.1mM KDP, pH=6.5 and IS=0.04M). The supersaturation was increased by adding 0.1mM and .05 mM aliquots of CaCl_2 , respectively.

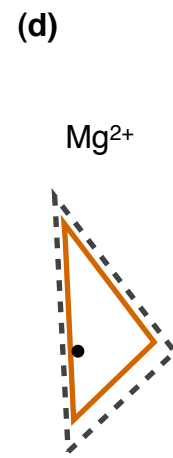
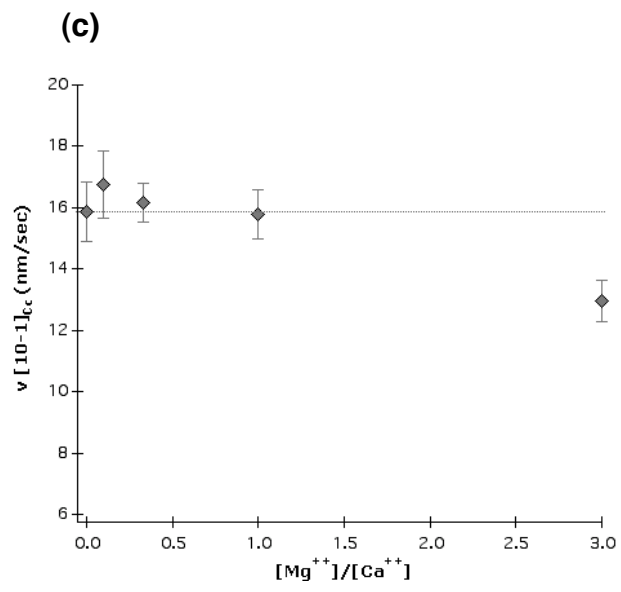
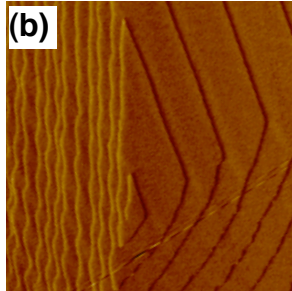
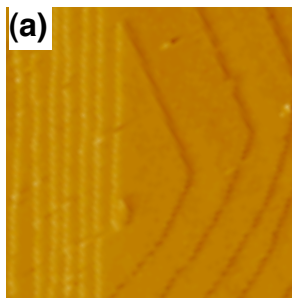


Figure 4

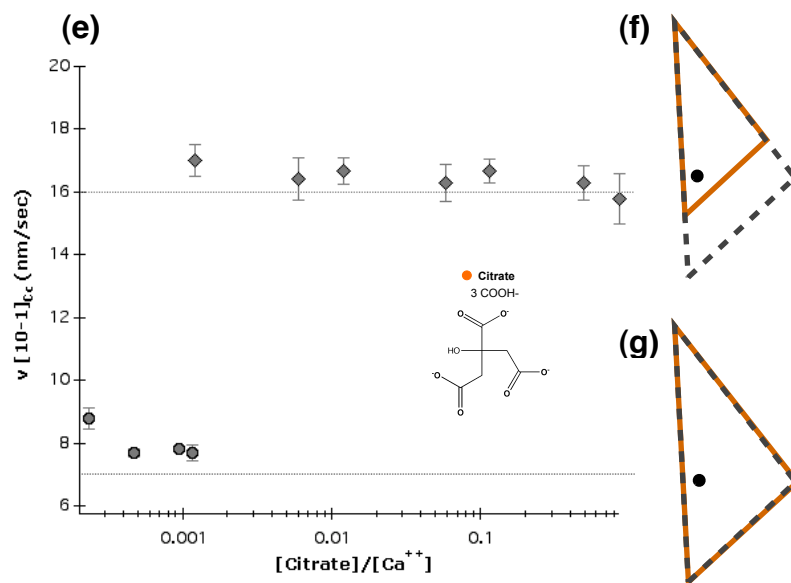
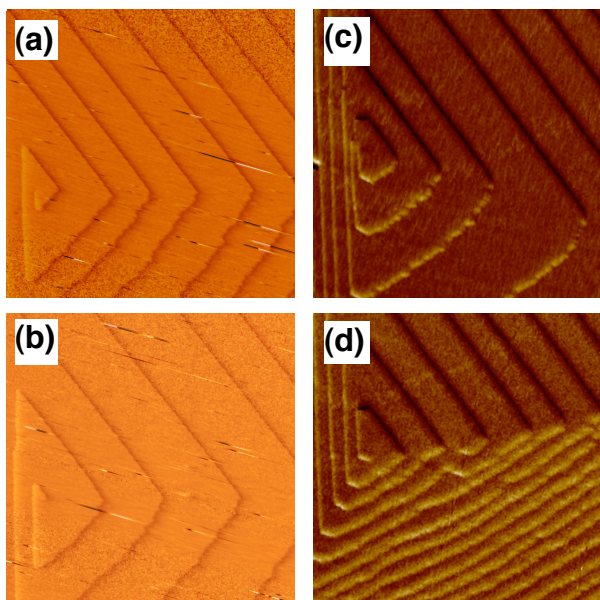


Figure 5

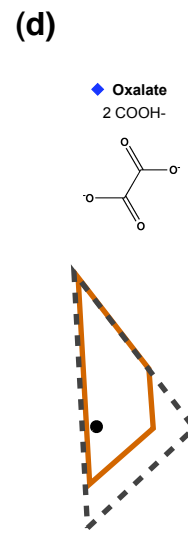
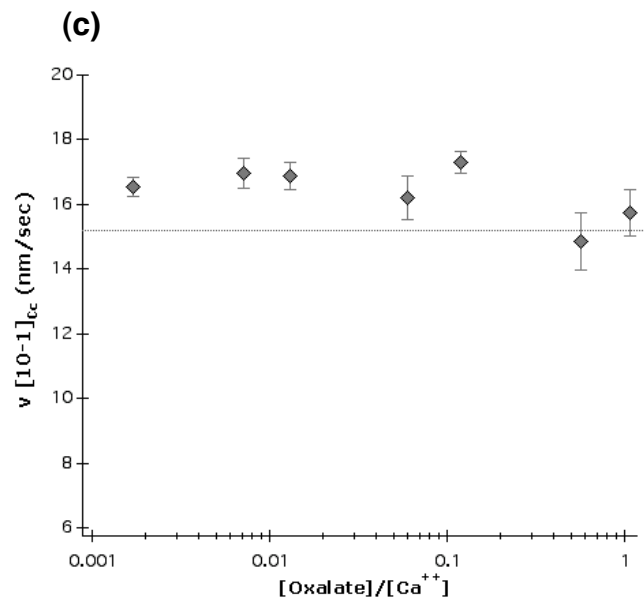
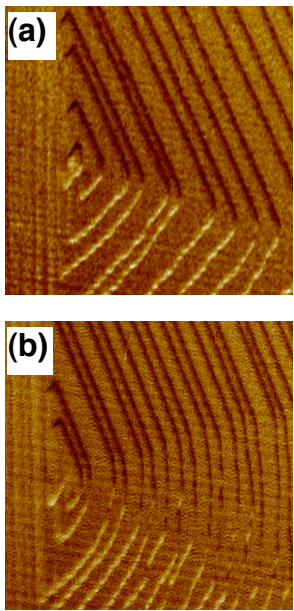


Figure 6

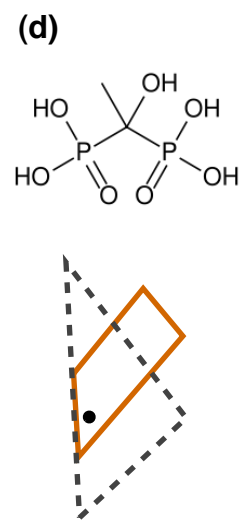
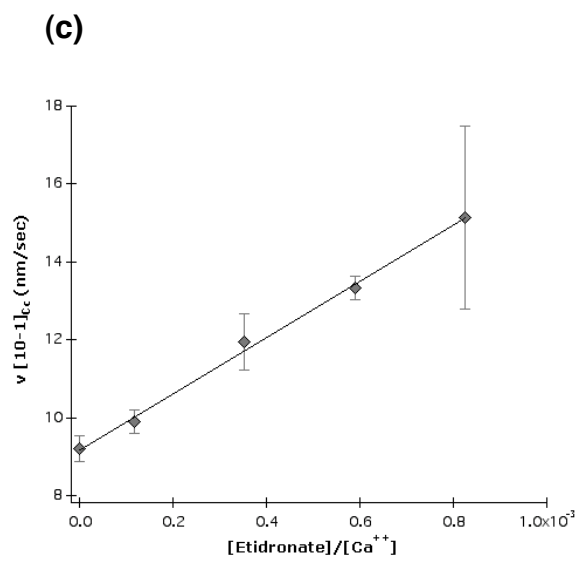
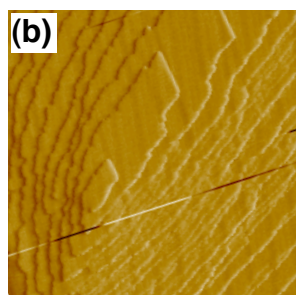
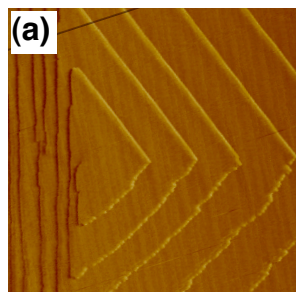


Figure 7

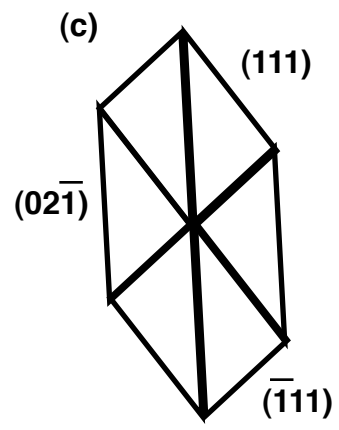
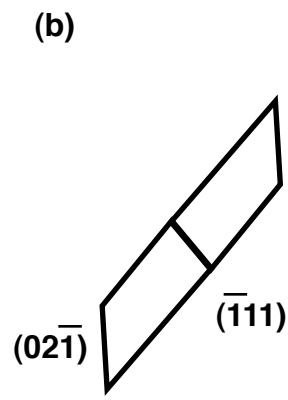
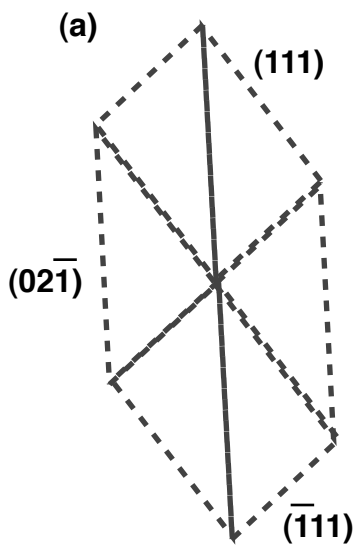


Figure 8